scientific reports

Check for updates

OPEN

Construction and validation of a cell based reporter assay for identifying inhibitors of SARS coronavirus 2 RNA dependent RNA polymerase activity

Eunjeong Kang[1,6], Haelim Yoon[1,6], Junho Lee[1], JinAh Lee[2], Seungtaek Kim[2], Inseong Jo[3], Soo Bong Han[3,4], Dae Gwin Jeong[5] & Sayeon Cho[1]✉

Targeting RNA-dependent RNA polymerase (RdRp), a highly conserved enzyme essential for SARS coronavirus 2 (SARS-CoV-2) replication and transcription, represents a promising antiviral strategy due to its lower mutation rate than structural proteins such as Spike. This study introduces a cell-based assay system for screening potential SARS-CoV-2 RdRp inhibitors, contributing to ongoing efforts to identify effective antiviral agents. The assay utilizes a reporter vector containing the 3′ untranslated region (UTR), luciferase reporter gene, and 5′ UTR gene, sequentially arranged in reverse under the control of the cytomegalovirus promoter in the pcDNA3.1 vector. Co-transfection with SARS-CoV-2 RdRp resulted an increase in luminescence-based quantification of RdRp activity, achieving a Z-factor of 0.605, indicative of high reproducibility and reliability for high-throughput screening. Established RdRp inhibitors, including remdesivir, molnupiravir, tenofovir, and sofosbuvir, significantly reduced reporter activity, with remdesivir exhibiting the strongest inhibition. A newly identified RdRp inhibitor was further validated through primer extension polymerase and NMPylation assays, along with virus-based experiments, confirming its inhibitory mechanism. These results highlight the utility of this screening system in identifying effective RdRp-targeting antivirals, reinforcing the strategic importance of RdRp inhibition in combating SARS-CoV-2 and emerging variants.

Keywords SARS-CoV-2, RdRp, High-throughput screening, Cell-based reporter assay, SARS-CoV-2 RdRp inhibitor

Severe Acute Respiratory Syndrome Coronavirus 2 (SARS-CoV-2) emerged in late 2019 in China, leading to the global COVID-19 pandemic[1]. This novel betacoronavirus, belonging to the *Coronaviridae* family and closely related to SARS-CoV and Middle East respiratory syndrome coronavirus, has a high potential for zoonotic transmission[2]. Beyond its respiratory impact, SARS-CoV-2 can cause pneumonia-like symptoms in the lower respiratory system and, in severe cases, multiple organ failure, potentially leading to death[3]. The ongoing global crisis underscores the urgent need for more dependable and expedient methods to identify asymptomatic SARS-CoV-2 infections.

SARS-CoV-2, a positive single-stranded ribonucleic acid (RNA) virus with a genome of approximately 30 kb, comprises 14 open reading frames (ORFs) that encode two main categories of proteins[4]. Roughly one-third of its genome codes for four structural proteins: spike, envelope, membrane, and nucleocapsid (N), along with six accessory proteins[5]. The remaining two-thirds of the genome encodes non-structural proteins (Nsps) located within the 5′-region of the viral RNA genome[5]. These Nsps are produced as two large polyproteins,

[1]Laboratory of Molecular and Pharmacological Cell Biology, College of Pharmacy, Chung-Ang University, Seoul 06974, Republic of Korea. [2]Zoonotic Virus Laboratory, Institut Pasteur Korea, Seongnam 13488, Republic of Korea. [3]Infectious Diseases Therapeutic Research Center, Korea Research Institute of Chemical Technology, Daejeon 34114, Republic of Korea. [4]Medicinal Chemistry and Pharmacology, University of Science and Technology, Daejeon 34113, Republic of Korea. [5]Bionanotechnology Research Center, Korea Research Institute of Bioscience and Biotechnology, Daejeon 34141, Republic of Korea. [6]These authors contributed equally to this work: Eunjeong Kang and Haelim Yoon. ✉email: sycho@cau.ac.kr

ORF1a and ORF1ab, which are subsequently cleaved into 16 smaller peptides (Nsp1-16) by main and papain-like proteases[5,6]. Nsps play crucial roles in various viral processes, including RNA replication and modification, synthesis of viral proteins, and the assembly of viral replicase complexes[7].

One of the most important components of the SARS-CoV-2 genome in viral replication is the RNA-dependent RNA polymerase (RdRp), also known as Nsp12[8]. SARS-CoV-2 RdRp comprises two essential domains: the N-terminal nidovirus RdRp-associated nucleotidyltransferase (NiRAN) domain, featuring a pseudokinase, and the C-terminal RdRp domain, which further divides into fingers, palm, and thumb subdomains[9]. The catalytic sites of NiRAN and RdRp domains are spatially separated by an interface domain[10]. The NiRAN domain is essential for transferring nucleotide monophosphates (NMPs) from nucleotide triphosphates to Nsp9, a key step in viral RNA synthesis[11]. The RdRp domain facilitates the transcription and replication of the viral RNA genome[12]. The combined activities of these domains play a critical role in the viral replication process. Importantly, RdRp exhibits a higher degree of conservation within the SARS-CoV-2 genome in terms of the number of mutations per residue compared to structural proteins such as spike and nucleocapsid, making RdRp a highly promising target for COVID-19 treatment strategies[13].

The process of RNA replication in SARS-CoV-2 relies on the replication and transcription complex (RTC), primarily composed of Nsp7, Nsp8, and SARS-CoV-2 RdRp[14]. Nsp7 and Nsp8 subunits bind to the thumb part of the RdRp domain, with an additional copy of Nsp8 attaching to the fingers[15]. This orchestrated collaboration significantly enhances the efficiency of RdRp during replication. Notably, remdesivir and molnupiravir, Food and Drug Administration (FDA)-approved drugs for COVID-19, specifically target RdRp, acting as inhibitors to impede its activity[16–18]. Additionally, other FDA-approved drugs, such as sofosbuvir, favipiravir, and tenofovir, have been shown to incorporate into RNA by SARS-CoV-2 RdRp, leading to the blockage of polymerase extension or RNA replication[19–22]. Efficient RNA synthesis is crucial for viral propagation, making the RNA replication machinery a compelling target for antiviral drug development.

Although various cell-based reporter screening methods have been proposed[8], the current state of therapeutic drug discovery for COVID-19 remains insufficient. There is an urgent need for a cost-effective and reliable high-throughput screening (HTS) assay to identify effective inhibitors, particularly those targeting RdRp. To address this need, we have established and optimized a cell-based reporter vector directly regulated by the activity of SARS-CoV-2 RdRp. Using this system, we identified a compound that inhibits both reporter activity and viral replication. Identifying such compounds through this reporter system is essential for combating SARS-CoV-2 and contributes to the ongoing search for targeted and impactful therapeutic interventions.

Results

Development of the cell-based SARS-CoV-2 reporter assay to measure SARS-CoV-2 RdRp activity

A luciferase reporter assay system was developed to assess intracellular SARS-CoV-2 RdRp enzyme activity. The reporter vector in this study is engineered with a reverse firefly luciferase (FLuc) gene, designed to be influenced by RdRp on the 5′ untranslated region (UTR) of SARS-CoV-2 (Fig. 1a). The 5′ UTR and 3′ UTR sequences of SARS-CoV-2, positioned on either side of FLuc, are arranged in reverse within two hepatitis delta virus (HDV) ribozyme self-cleavage sequences. Reporter activity is initiated by RNA transcription triggered by the host RNA polymerase II from the cytomegalovirus (CMV) promoter (Fig. 1b). The resulting RNA transcript undergoes self-cleavage via the ribozyme, leading to the expression of negatively oriented 3′ UTR-FLuc-5′ UTR RNA. Subsequently, forward FLuc RNA is transcribed by RdRp, facilitating FLuc expression. Consequently, in cells transfected with the reporter vector, FLuc signal intensity is modulated based on the level of transiently expressed RdRp. Therefore, in this study, reporter activity is represented by FLuc values.

Verification and optimization of the cell-based reporter assay

To evaluate the regulation of reporter activity by SARS-CoV-2 RdRp, the reporter vector and RdRp were expressed at ratios of 1:1, 1:2, and 1:4 (Fig. 2a). The activity of the reporter exhibited a significant dose-dependent increase with various doses of RdRp. The dose-dependent transfection efficiency of RdRp was confirmed through immunoblotting (Supplementary Fig. S1a). Subsequent experiments determined that a 1:4 ratio of the reporter vector to RdRp consistently resulted in the highest peak of reporter activity. These experimental conditions did not affect cell viability for 72 h, but only regulated reporter activity, regardless of whether the reporter vector was expressed alone or co-expressed with RdRp (Supplementary Fig. S1b). Nsp7 and Nsp8 collaboratively form the RTC with RdRp to stabilize the RNA binding region[9]. To assess the significance of Nsp7 and Nsp8 in the cell-based reporter assay, they were co-expressed with RdRp in human embryonic kidney (HEK) 293 cells expressing the reporter vector (Fig. 2b). RdRp, Nsp7, and Nsp8 were transiently expressed in HEK 293 cells, as confirmed by immunoblotting (Supplementary Fig. S1c). The addition of RdRp resulted in a significant increase in reporter activity. However, the addition of Nsp7 and Nsp8 did not significantly augment reporter activity compared to the group transfected only with RdRp.

Considering that SARS-CoV-2 mainly causes respiratory infections, the A549 cell line, derived from human lung alveolar epithelial cells, is used as a suitable model in various studies related to SARS-CoV-2[23,24]. In this study, the reporter assay, initially conducted in HEK 293 cells, was extended to A549 cells for further validation. In A549 cells expressing the reporter vector, a significant increase in reporter activity was observed upon expression of RdRp. Similarly to HEK 293 cells, Nsp7 and Nsp8 did not demonstrate significant effect in A549 cells (Supplementary Fig. S2a). The results exhibited the same tendency as in HEK 293 cells.

To determine the optimal time for maximizing reporter activity following RdRp transfection, HEK 293 cells were co-transfected with the reporter vector and RdRp at the previously verified optimal ratio of 1:4 (Fig. 2c).

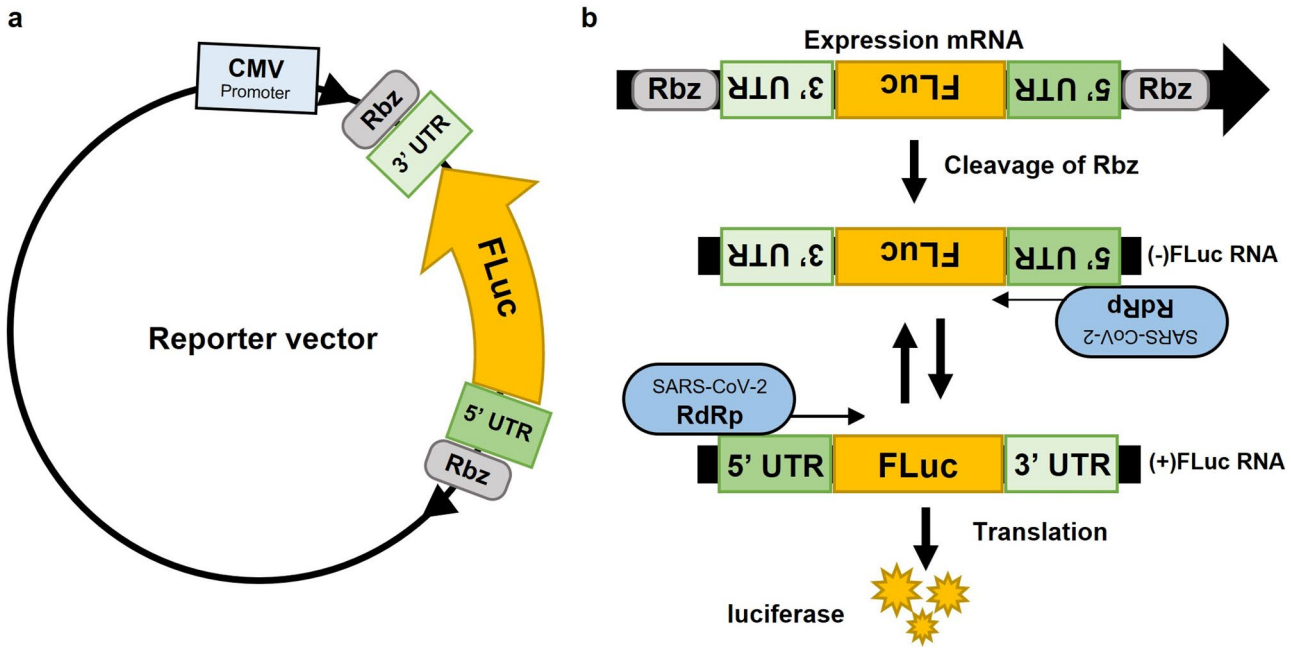

Fig. 1. Schematic diagram of the cell-based reporter assay system. (**a**) Reporter vector was engineered to measure the activity of SARS-CoV-2 RdRp by regulating FLuc under the control of the 5′ UTR. This reporter plasmid incorporates the FLuc gene between the 5′ UTR and 3′ UTR of SARS-CoV-2 in the reverse orientation, following the CMV promoter. (**b**) The RNA transcript, driven by the CMV promoter, undergoes ribozyme-mediated cleavage at both ends, producing the 5′ UTR-FLuc-3′ UTR RNA transcript. RdRp recognizes the 5′ UTR, initiates RNA polymerization, and transcribes FLuc in the positive direction. The level of FLuc transcribed by RdRp is quantified and expressed as the reporter activity value. The ribozyme is denoted as Rbz in both diagrams.

Comparing reporter activity between groups with and without RdRp revealed a significant increase at least 24 h post-transfection, peaking at 48 h and gradually decreasing thereafter.

The major domains that regulate the polymerase activity of SARS-CoV-2 RdRp include the NiRAN domain in the N-term and the RdRp domain in the C-term. To further verify the activation of the reporter vector by RdRp, we evaluated reporter activity with mutations in key residues in the NiRAN domain (Lys73 and Asp218) and RdRp domain (Asp618, Asp760, and Asp761). These residues were mutated to Ala to inactivate RdRp. As shown in Fig. 2d, mutants of RdRp exhibited a significant decrease in reporter activity compared to the wild type (WT) of RdRp. However, the group with a triple mutation targeting the RdRp domain (Asp618, Asp760, and Asp761) showed a dramatic reduction in reporter activity. This suggests that the RdRp domain of SARS-CoV-2 RdRp plays a crucial role in the activation of the reporter assay.

Evaluation of reliability and reproducibility of reporter analysis

Before screening for SARS-CoV-2 RdRp inhibitors using the constructed reporter vector, we validated the reporter assay by calculating the Z-factor, an indicator of reproducibility and reliability. The Z-factor was determined by introducing RdRp into HEK 293 cells expressing the reporter vector (Fig. 3). Additionally, the Z′-factor was calculated by assessing how remdesivir, a positive control known for targeting SARS-CoV-2 RdRp polymerase activity, modulated reporter activity. The Z-factor was computed as 0.605, and the Z′-factor as 0.601. The Z-factor, which ranges from − 1 to 1, indicates the quality of the screening system, with higher values suggesting better quality. Typically, a value exceeding 0.5 is considered indicative of a reliable screening system. Therefore, the calculated Z-factor of 0.605 supports that screening using the reporter is both reproducible and reliable.

Effect of RdRp inhibitors on reporter activity

In the preceding experiment, we established optimal conditions for analyzing RdRp activity with the designated reporter vector and verified the reliability of this analysis in both HEK 293 and A549 cells. Before conducting HTS of an inhibitor library, we aimed to demonstrate the efficacy of the reporter assay under optimized conditions using various FDA-approved drugs and compounds proposed as potential RdRp inhibitors. As shown in Fig. 4a, remdesivir, a widely used COVID-19 treatment[25], significantly inhibited reporter activity, with an IC_{50} value of 3.7 μM in HEK 293 cells and 2.7 μM in A549 cells, respectively. Molnupiravir, another drug used for SARS-CoV-2 treatment, is an oral prodrug of the ribonucleoside beta-D-N4-hydroxycytidine (NHC)[26]. Molnupiravir exhibited an IC_{50} value of 7.3 μM in HEK 293 cells and 3.8 μM in A549 cells, indicating lower potency in modulating RdRp activity compared to remdesivir (Fig. 4b). Tenofovir and sofosbuvir, prescribed

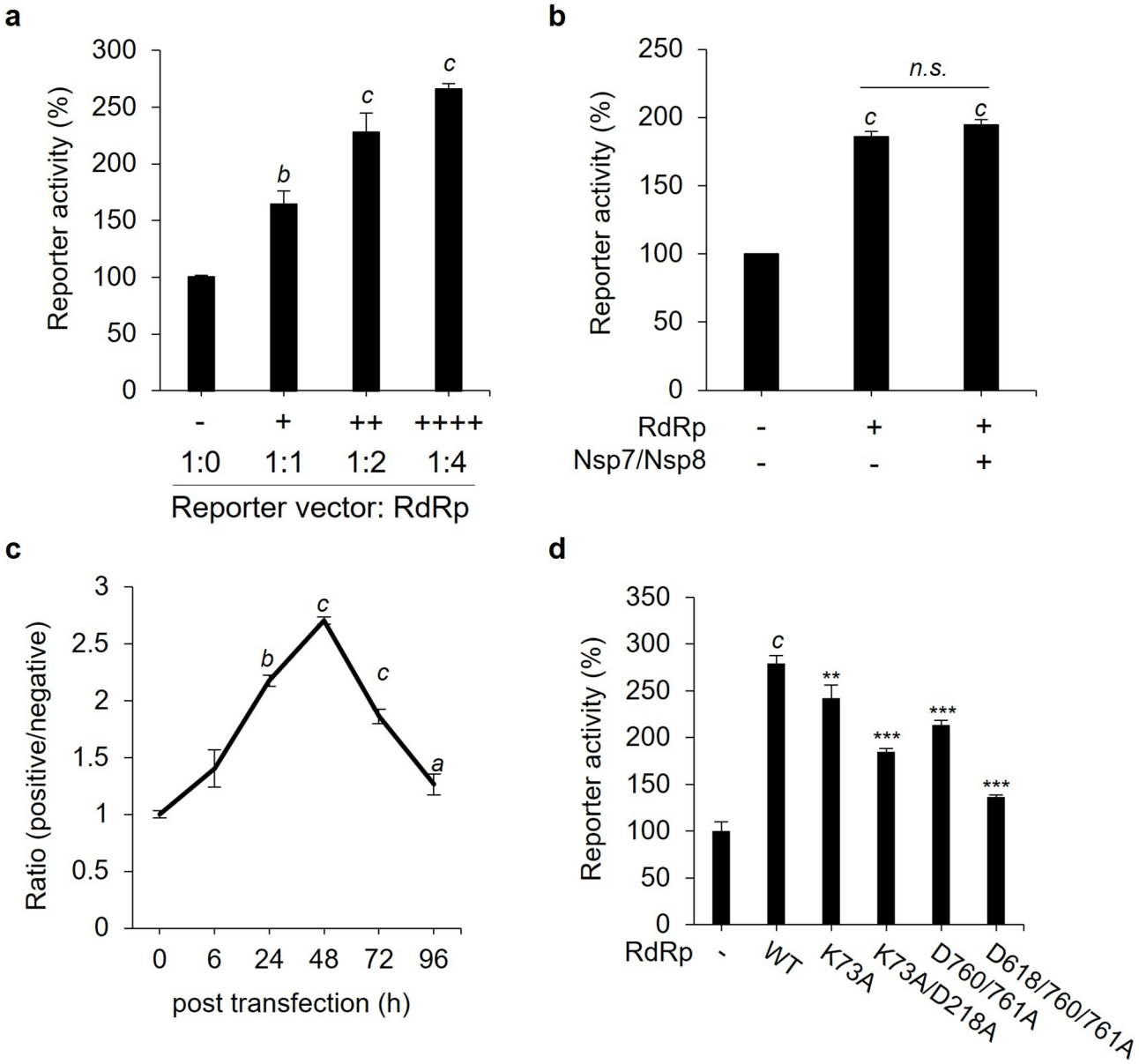

Fig. 2. Confirmation of reporter activity through expression of SARS-CoV-2 RdRp. (**a**) HEK 293 cells were co-transfected with our constructed reporter vector and RdRp at various ratios (1:1, 1:2, and 1:4). Reporter activity was evaluated after 48 h of incubation. (**b**) Reporter activity was compared between the single expression of RdRp and the co-expression of Nsp7, Nsp8, and RdRp in reporter-transfected HEK 293 cells. (**c**) The expression of the reporter vector was assessed at various time intervals following the transfection of HEK 293 cells with RdRp. The reporter activity value of the reporter vector and RdRp co-expression group was divided by the reporter activity value of the reporter vector expression group and expressed as a ratio. (**d**) Reporter activity was measured following the mutation of essential residues Lys73 and Asp218 (depicted as K73 and D218) in the NiRAN domain of RdRp, or the mutation of key residues Asp618, Asp760, and Asp761 (depicted as D618, D760, and D761) in the RdRp domain of RdRp. Each key residue that regulates the activity of SARS-CoV-2 was replaced with alanine, indicated as 'A' in the graph. All data on reporter activity are expressed as a percentage compared to the reporter expression group. The data represent the results of three independent experiments. Statistical significance is indicated as follows: $^{a}p < 0.05$, $^{b}p < 0.01$, and $^{c}p < 0.001$ compared to the reporter vector expressed group; $^{**}p < 0.01$ and $^{***}p < 0.001$ compared to the reporter vector and RdRp co-expressed group; *n.s.*, non-significant.

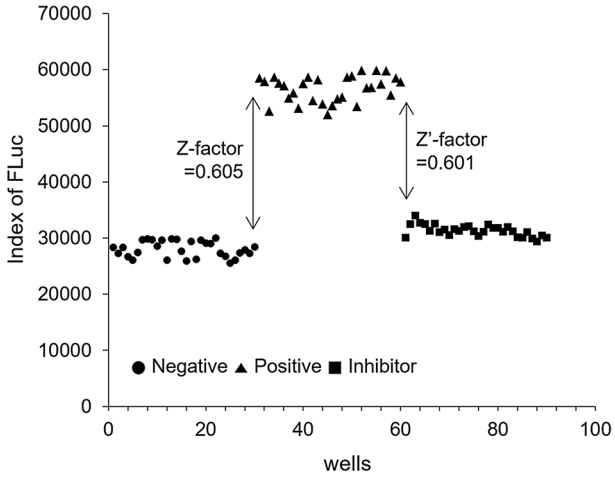

Fig. 3. Evaluation of a cell-based reporter assay system for HTS using Z-factor analysis. The experimental groups included a negative control group (reporter vector expression group; (●), a positive control group (reporter vector and RdRp co-expression group; (▲), and an RdRp inhibitor treatment group (positive group treated with remdesivir; 5 μM for 24 h; (▪) in HEK 293 cells expressing the reporter. Positive and negative controls were treated with DMSO instead of remdesivir. Z- and Z′-factors were calculated using Zhang's formula for each group: negative, positive, and inhibitor.

for hepatitis virus infections, are suggested to bind to SARS-CoV-2 RdRp[27]. In HEK 293 cells, tenofovir and sofosbuvir showed IC_{50} values of 8.0 μM and 7.3 μM, respectively, while in A549 cells, the values were 9.9 μM and 6.2 μM, respectively (Fig. 4c and d). Among the four compounds assessed, remdesivir was identified as the most effective in reducing reporter activity, affirming the utility of the reporter assay for discovering inhibitors of SARS-CoV-2 RdRp activity.

Screening to discover a compound that inhibits the activity of RdRp

Given the kinase-like activity associated with the NiRAN domain of SARS-CoV-2 RdRp[28], several studies suggest that compounds inhibiting kinase activity may serve as RdRp inhibitors[29,30]. In this study, a library of kinase-inhibiting compounds from the Korea Chemical Bank (KCB) was used in a cell-based reporter assay for HTS of SARS-CoV-2 RdRp inhibitors. HEK 293 cells co-expressing the reporter vector and RdRp were treated with 2,704 compounds to identify those inhibiting RdRp activity. As illustrated in Fig. 5a, the screening data were displayed as a heatmap, which was initially performed in HEK 293 cells co-expressing the reporter vector and RdRp. Based on this heatmap, we identified [4-[1-(2-methylphenyl)tetrazol-5-yl]sulfanyl-3-nitrophenyl]-phenylmethanone (MePT-S-N-PMe) as the compound exhibiting the lowest IC_{50} value for inhibiting reporter activity. The structure of MePT-S-N-PMe is shown in Fig. 5b and demonstrated a significant reduced reporter activity with an IC_{50} value of 7.0 μM in HEK 293 cells without affecting cell viability (Fig. 5c). Furthermore, MePT-S-N-PMe significantly suppressed reporter activity in A549 cells with an IC_{50} value of 3.8 μM (Supplementary Fig. S2b), indicating effective inhibition in both HEK 293 and A549 cells.

Given that MePT-S-N-PMe reduced reporter activity in cells, a primer extension polymerase assay involving the SARS-CoV-2 RTC, adenosine triphosphate (ATP), and an RNA primer-template pair was conducted to determine its direct effect on RdRp activity in vitro (Fig. 5d). In the presence of these components, MePT-S-N-PMe significantly inhibited RdRp activity in a dose-dependent manner, leading to the termination of RNA synthesis. Since RdRp contains both the RdRp domain and the NiRAN domain, we also investigated whether MePT-S-N-PMe affects the function of the NiRAN domain by examining the NiRAN-mediated transferase activity using an NMPylation assay (Fig. 5e). The protein expression of SARS-CoV-2 Nsp9 and RdRp was confirmed via Coomassie blue staining (Supplementary Fig. S3). Although the NMPylation effect was less pronounced at the concentrations used in the primer extension polymerase assay, the highest concentration of MePT-S-N-PMe (50 μM) appeared to exhibit a slight inhibitory effect on nucleotidyltransferase activity. Taken together, MePT-S-N-PMe effectively inhibited luciferase activity in HEK 293 and A549 cells transfected with the reporter vector and RdRp by regulating the polymerase activity of RdRp.

Antiviral effect of MePT-S-N-PMe in Vero and A549-hACE2-TMPRSS2 cells

The antiviral efficacy of MePT-S-N-PMe against SARS-CoV-2 was evaluated using immunofluorescence with an antibody targeting the N protein in SARS-CoV-2-infected Vero cells. Vero cells are commonly employed in viral infection studies due to their deficiency in interferon production, which enables high-titer replication of SARS-CoV-2[31]. As shown in Fig. 6a, treatment with MePT-S-N-PMe significantly inhibited SARS-CoV-2 replication, as evidenced by the reduced fluorescence of the immunostained SARS-CoV-2 N protein compared to the untreated group. The quantitative analysis demonstrated that the IC_{50} value for SARS-CoV-2 replication inhibition is 8.2 μM, following MePT-S-N-PMe treatment, without affecting cell viability (Fig. 6b). To further evaluate its antiviral efficacy of MePT-S-N-PMe in human lung cells, A549-hACE2-TMPRSS2, which are a human lung epithelial cell

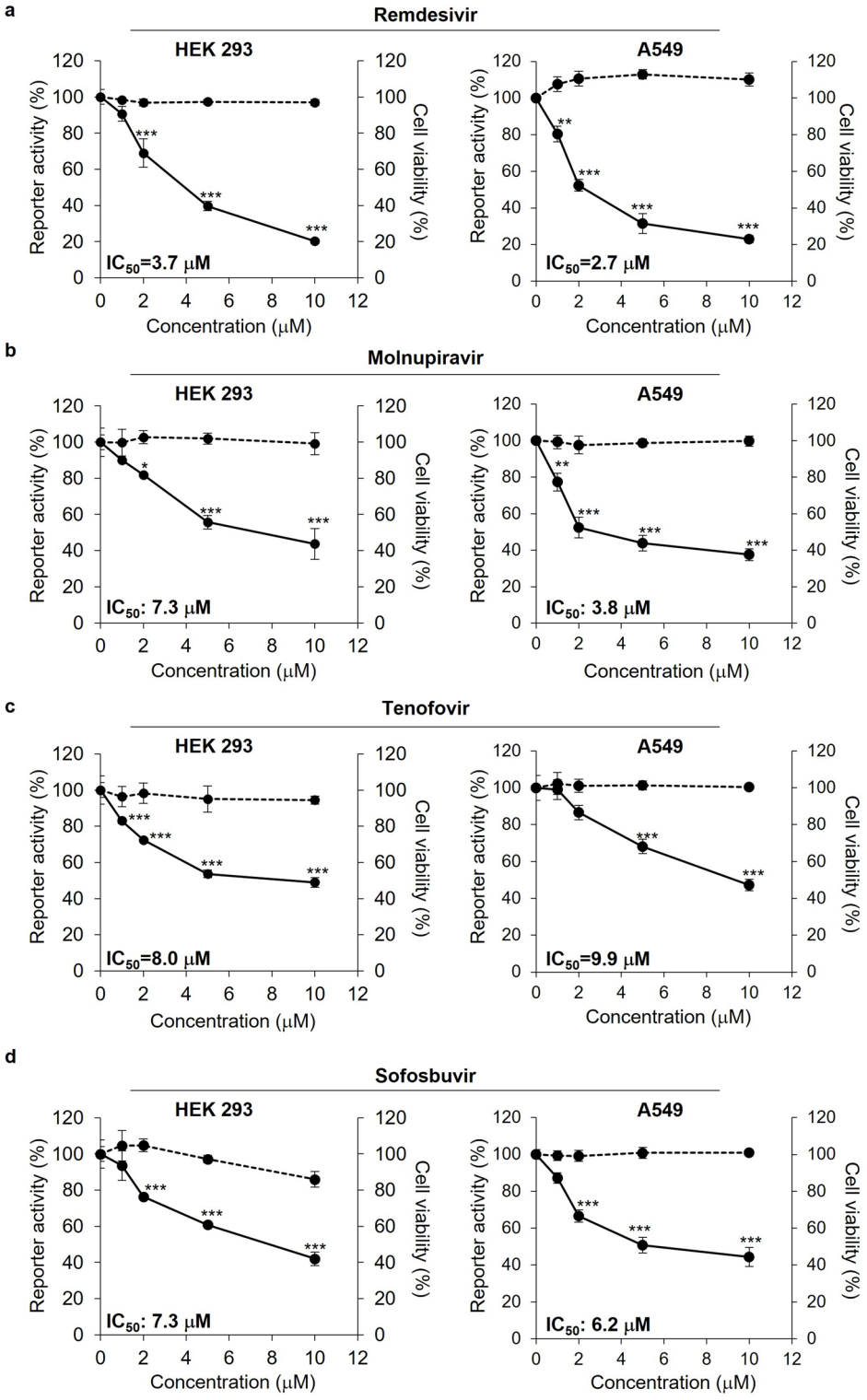

Fig. 4. Validation of reporter assay using inhibitors of SARS-CoV-2 RdRp activity. HEK 293 cells and A549 cells were transiently transfected with the reporter vector and RdRp. After 24 h, the cells were treated with various concentrations of (**a**) remdesivir, (**b**) molnupiravir, (**c**) tenofovir, and (**d**) sofosbuvir. These compounds were added to the reporter vector and RdRp co-expressed cells, followed by an additional 24 h incubation to measure reporter activity (solid line) and cell viability (dotted line). The data represent the results of three independent experiments. Reporter activity was expressed as a percentage relative to the reporter and RdRp co-expressed group. Statistical significance is denoted as $^{*}p < 0.05$, $^{**}p < 0.01$, and $^{***}p < 0.001$ compared to the reporter vector and RdRp co-expressed group.

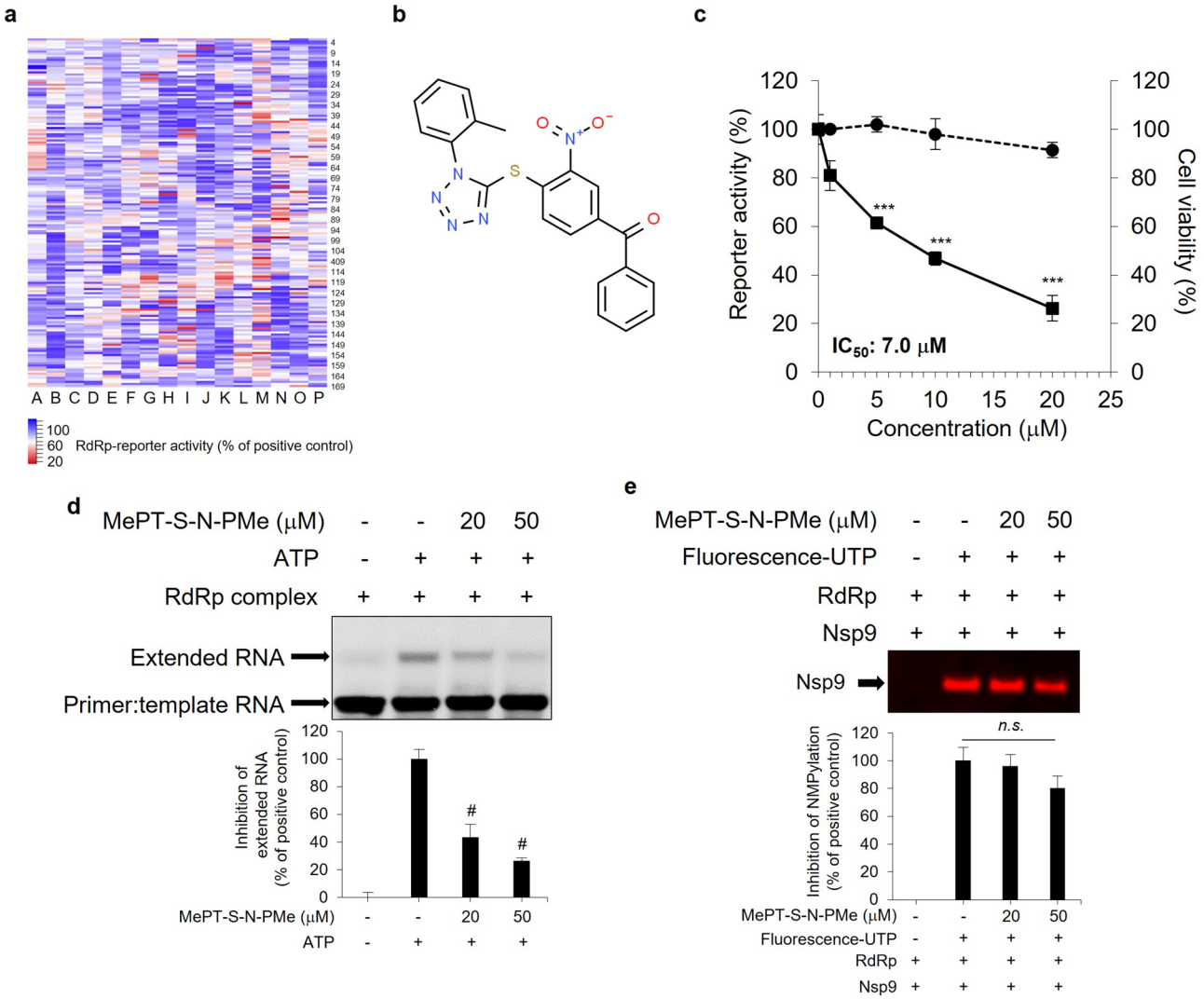

Fig. 5. Screening of compounds inhibiting SARS-CoV-2 RdRp activity using our constructed reporter vector. (**a**) A heatmap illustrating the regulation of reporter activity following treatment with 2,704 kinase inhibitors. HEK 293 cells co-transfected with Reporter and RdRp were treated with DMSO or 10 μM of test compounds for 24 h. Luminescence was measured using a reporter assay kit. Reporter values were compared to the positive control group (the reporter vector and RdRp co-expressed group) and expressed as a percentage of reporter activity. (**b**) Chemical structure of MePT-S-N-PMe. (**c**) HEK 293 cells expressing reporter vector and RdRp were treated with MePT-S-N-PMe for 24 h. The inhibition rate of RdRp activity by MePT-S-N-PMe at various concentrations was determined using a reporter assay kit, while cytotoxicity was assessed using EZ-Cytox. Reporter activity and cell viability are represented as a solid line and a dotted line, respectively. Results are presented as percentages relative to the reporter vector and RdRp co-expressed group, based on three independent experiments conducted in triplicate. (**d**) The primer extension reaction was initiated by treating the active SARS-CoV-2 RdRp complex and an annealed primer-template with MePT-S-N-PMe (20 and 50 μM) and ATP (50 μM). The reaction was carried out at room temperature for 1 h and then terminated by adding 2× RNA loading dye. The positive control group contained only ATP in the RdRp complex and the annealed primer-template. (**e**) For nucleotidyltransferase activity analysis, MePT-S-N-PMe (20 and 50 μM) was incubated with 0.5 μM of recombinant SARS-CoV-2 RdRp His-tag protein at 4 °C for 1 h. Subsequently, 5 μM purified Nsp9 and a UTP mixture (1.7 μM Fluorescein-12-UTP and 25 μM UTP) were added and incubated at room temperature for an additional 30 min. The reacted proteins were separated on a 12% SDS-PAGE gel, and fluorescence emitted from Nsp9 was visualized using a fluorescence detector. $^{*}p < 0.05$ and $^{***}p < 0.001$ compared to the reporter vector and RdRp co-expressed group; $^{\#}p < 0.05$ compared to the group treated with ATP and the RdRp complex; *n.s.*, non-significant.

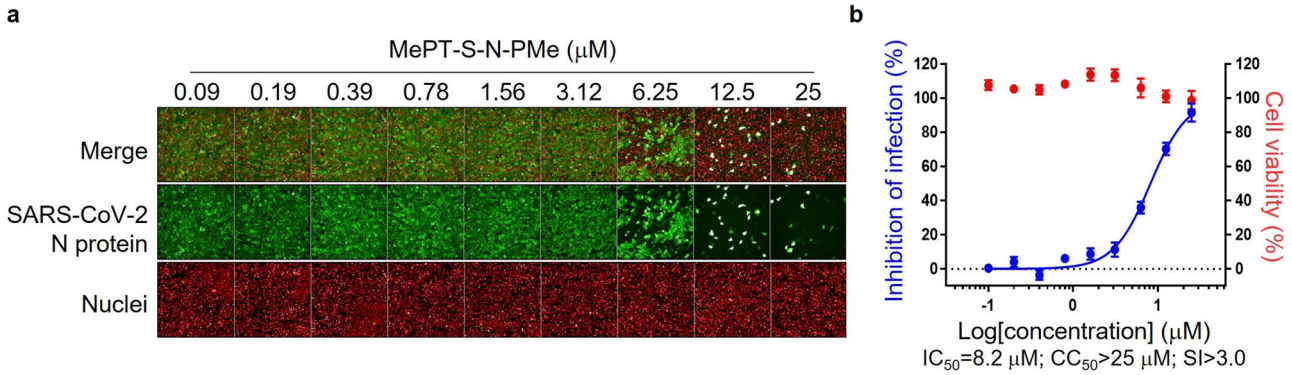

Fig. 6. Inhibition of viral replication by MePT-S-N-PMe in Vero cells. (**a**) Vero cells were treated with varying concentrations of MePT-S-N-PMe and then inoculated with the SARS-CoV-2 virus. After 24 h, cells were fixed with 4% paraformaldehyde and visualized by immunostaining for nuclei and nucleocapsid (N) protein of SARS-CoV-2. (**b**) The inhibition of SARS-CoV-2 infection (blue) and cell viability (red) were calculated as percentages compared to the untreated group and expressed as graphs. Mean ± standard deviation was calculated from duplicate experiments.

line stably expressing human angiotensin-converting enzyme 2 (ACE2) and transmembrane serine protease 2 (TMPRSS2) were used. In this model, MePT-S-N-PMe exhibited an IC_{50} value of 25.3 μM without affecting cell viability (Supplementary Fig. S4a). As the positive control, remdesivir showed potent antiviral activity, with IC_{50} values of 2.3 μM in Vero cells and 0.1 μM in A549-hACE2-TMPRSS2 cells (Supplementary Fig. S4b). Collectively, these results demonstrate that MePT-S-N-PMe effectively suppresses SARS-CoV-2 replication in both Vero and A549-hACE2-TMPRSS2 cells, with greater potency observed in Vero cells.

Discussion

As RdRp is a critical protein in the replication of SARS-CoV-2[12], efficient HTS systems are urgently needed to accelerate drug discovery targeting SARS-CoV-2 RdRp. To achieve this goal, we constructed an RdRp-dependent cell-based reporter vector that mimics viral replication.

Various cell-based assays measuring RdRp activity have consistently shown that the RdRp enzyme, when associated with the 5′ UTR of negative-sense genomic RNA, facilitates the production of positive-sense RNA[16,32–35]. In this study, we anticipated that the reporter vector would exhibit enhanced sensitivity to RdRp activity, irrespective of CMV promoter-driven expression. This sensitivity is due to the recognition of the 5′ UTR region of SARS-CoV-2 by RdRp, leading to the expression of FLuc RNA. To optimize the specificity and reliability of the system, self-cleaving ribozymes were inserted at both ends of the reporter cassette. This design ensures that transcripts generated from the CMV promoter are precisely cleaved, producing RNA with defined terminus. In addition, the reporter cassette was inserted in reverse orientation relative to the plasmid backbone. This design prevents background expression from plasmid-derived transcripts, as the reverse orientation of the luciferase gene precludes direct translation from host machinery. As a result, luciferase activity reflects only the RNA synthesized de novo by the RdRp. The functionality of the system was validated by measuring reporter activity in the presence or absence of RdRp. Comparing the reporter activity with and without RdRp 48 h post-transfection, the activity markedly increased by approximately 2.5-fold. The main domains of SARS-CoV-2 RdRp, the NiRAN domain and the RdRp domain, are critical for RNA polymerase activity[36]. Based on various in vitro and in silico studies, residues at Lys73 and Asp218 within the NiRAN domain, as well as residues at Asp618, Asp760, and Asp761 within the RdRp domain, are pivotal for viral replication[37,38]. In this study, individual or collective mutations of these residues in the NiRAN and RdRp domains resulted in reduced reporter activity compared to the RdRp WT. Among these mutations, the double amino acid mutation in the NiRAN domain and the triple amino acid mutation in the RdRp domain exhibited a pronounced reduction in reporter activity. This observation suggests that simultaneous mutation of these amino acids effectively inhibits the polymerase activity of RdRp.

Several FDA-approved RdRp inhibitors, such as remdesivir and molnupiravir, along with potent RdRp inhibitors undergoing preclinical or clinical studies, including tenofovir and sofosbuvir, are being investigated for COVID-19 treatment[22]. Originally employed in treating Ebola virus[39], remdesivir is now FDA-approved for COVID-19 treatment, with numerous studies demonstrating its potent inhibition of SARS-CoV-2 replication by targeting SARS-CoV-2 RdRp in vitro[40–43]. In our cell-based reporter assay, remdesivir exhibited the lowest IC_{50} value compared to other inhibitors, indicating its superior potency against reporter activity. Molnupiravir, which has received emergency use authorization from the FDA for mild-to-moderate COVID-19[44], exhibited the second-highest inhibition of reporter activity. According to a study by Kabinger et al., the active form of molnupiravir in cells, NHC triphosphate, incorporates NHC monophosphate into RNA, leading to mutations in the final RNA products[45]. Additionally, tenofovir and sofosbuvir, which are FDA-approved for inhibiting the polymerase of hepatitis viruses[46,47], have been computationally predicted to bind to SARS-CoV-2 RdRp[30]. Known for their ability to enhance antiviral activity by inhibiting exonuclease activity, these compounds also displayed

inhibitory effects on SARS-CoV-2 replication[22,48]. Although their inhibitory magnitude was not as pronounced as remdesivir, both compounds exhibited a dose-dependent reduction in reporter activity. The observed decrease in reporter activity induced by remdesivir, molnupiravir, tenofovir, and sofosbuvir confirms the effective mimicry of viral replication by the reporter vector and RdRp. However, nucleoside analogs often exhibit poor solubility and limited membrane permeability due to the inefficiency of transmembrane nucleoside transporters, resulting in low bioavailability[49,50]. Additionally, nucleoside analogs typically require phosphorylation to become active antiviral agents, which is a rate-limiting step that can further constrain their efficacy[51]. Moreover, these drugs are associated with adverse side effects, including influenza-like illness, anaphylactic reactions, gastrointestinal disorders, and nervous system disorders[52–55]. Therefore, there is a critical need to develop drugs with fewer side effects for the treatment of SARS-CoV-2.

Given the significance of protein kinases as COVID-19 drug targets[56,57], our reporter assay that mimics SARS-CoV-2 replication used a kinase inhibitor library. Through HTS, MePT-S-N-PMe exhibited the most significant reduction in reporter activity. Treatment with MePT-S-N-PMe dose-dependently inhibited RNA synthesis in the primer extension polymerase assay, highlighting its potential to target SARS-CoV-2 RdRp. Additionally, MePT-S-N-PMe slightly inhibited the nucleotidyltransferase activity of RdRp, which is responsible for transferring NMP to the protein substrate Nsp9. Given the multifunctional role of the NiRAN domain, which includes RNA capping and RNA synthesis priming[58], this slight inhibition could further impede viral replication. It is plausible that MePT-S-N-PMe targets both the RdRp and NiRAN domains, potentially inhibiting downstream processes dependent on polymerase and nucleotidyltransferase activities. To further assess the antiviral potential of MePT-S-N-PMe, its efficacy was evaluated in SARS-CoV-2-infected cells. In both Vero and A549-hACE2-TMPRSS2 cells, MePT-S-N-PMe effectively suppressed viral replication without affecting cell viability. These findings support the functional relevance of the compound in cellular infection models and are consistent with its inhibitory effects observed in the reporter and polymerase assays. Notably, the observed differences in IC_{50} values across cell types may reflect variations in cellular uptake, metabolic capacity, host factor expression, or efflux transporter activity[59–61]. Additional factors such as the intrinsic characteristics of the host cell type, including receptor expression and intracellular signaling pathways, may further contribute to the observed discrepancies in drug efficacy[62–64]. Taken together, these findings position MePT-S-N-PMe as a candidate for further development as an antiviral agent targeting multiple enzymatic functions of SARS-CoV-2 RdRp. Although MePT-S-N-PMe is predicted to inhibit both RdRp and NiRAN domains, further investigations are needed to confirm its direct interaction with RdRp and to elucidate its precise antiviral mechanism.

Our constructed vector and HTS system had several limitations that need to be considered in depth. Nsp7 and Nsp8, as the co-factors of RTC, form a complex with RdRp, creating an active site, which is an RNA-template binding site, stabilizing the complex[65]. However, in our experiments, there was no significant difference between reporter activities with RdRp alone and with Nsp7 and Nsp8 together in both HEK 293 and A549 cells. Our results indicate that an increase in reporter activity can be observed solely with RdRp. Similarly, a study by Min et al. has shown that SARS-CoV-2 RdRp alone, independent of Nsp7 and Nsp8, can also lead to an increase in reporter activity[35]. This might be due to the presence of intracellular proteins within the cell mimicking Nsp7 and Nsp8, allowing RdRp to function even when transfected alone into cells. Supporting this hypothesis, an in silico study by Gordon et al. identified several human proteins, such as proline-rich coiled-coil 2B[66], as potential RdRp interactors, although their functional relevance remains unclear. These findings highlight the need for further investigation into the role of Nsp7 and Nsp8 within the context of the reporter vector. Despite these limitations, the high Z-factor of our reporter assay and antiviral effects observed in virus-infected cells support the reliability and reproducibility for screening SARS-CoV-2 RdRp inhibitors in HTS system. These findings underscore the effectiveness of our developed HTS system using the reporter vector in identifying potential inhibitors of SARS-CoV-2 RdRp.

In conclusion, our developed cell-based reporter vector, validated with known SARS-CoV-2 RdRp inhibitors such as remdesivir, demonstrates its effectiveness in mimicking viral replication in cells. Given the highly conserved domains within RdRp among coronaviruses and other RNA positive-stranded viruses, this platform may also be applicable to studying antivirals targeting these viral families. Moreover, its potential utility extends beyond human infections to animal coronaviruses, including those responsible for diseases such as feline infectious peritonitis, broadening the scope of antiviral drug discovery. The high reliability and reproducibility of our reporter assay also suggest its suitability for HTS approaches, expediting the discovery of effective therapeutic drugs for COVID-19 and its variants. In this study, although a single compound exhibiting inhibition of SARS-CoV-2 RdRp polymerase activity was identified from the library of kinase-inhibiting compounds, future efforts will involve utilizing our constructed reporter vector to screen a broader range of compound libraries with the goal of discovering additional promising antiviral agents.

Materials and methods

Chemical screening

A chemical compound library containing 2,704 kinase inhibitors was provided by the KCB (http://www.chembank.org). The library was screened using a reporter assay in HEK 293 cells. Heatmap analysis, performed using Heatmapper (http://www.heatmapper.ca/expression/), visualized the RdRp activity of compounds screened in the reporter assay. The reporter activity values in the heatmap were expressed as a ratio relative to the control group treated with dimethyl sulfoxide (DMSO) alone. Compounds with the potential to inhibit RdRp activity were indicated by lower reporter activity, visually represented in red on the heatmap. We conducted a literature search using the chemical structures of compounds provided by the KCB. Six candidates were chosen for further evaluation, as there were no previous reports on SARS-CoV-2-related reporter assays or viral replication associated with these compounds.

Cell culture

HEK 293 cells were purchased from the American Type Culture Collection (CRL-1573; ATCC, VA, USA), and A549 cells were purchased from the Korean Cell Line Bank (Seoul, Korea). Both HEK 293 and A549 cells were maintained in Dulbecco's Modified Eagle's Medium (DMEM) (WELGENE Inc., Gyeongsangbuk-do, Korea), supplemented with 10% fetal bovine serum (FBS) (WELGENE Inc., Gyeongsangbuk-do, Korea), and 1% penicillin/streptomycin (Gibco, MA, USA)[67,68]. Cells were cultured in a humidified incubator at 37 °C with 5% CO_2.

Plasmids, reagents, and antibodies

Strep-tagged plasmids including SARS-CoV-2 RdRp (plasmid #141378), Nsp7 (plasmid #141373), and Nsp8 (plasmid #141374) were obtained from Addgene (MA, USA). Rabbit polyclonal anti-Strep epitope tag (cat. No. GTX128061), rabbit polyclonal anti-GAPDH (cat. No. GTX100118), and goat polyclonal anti-rabbit IgG-HRP (cat. No. GTX213110-01) were purchased from GeneTex, Inc. (CA, USA). Remdesivir (HY-104077) was purchased from MedChemExpress (NJ, USA). Molnupiravir (EIDD-2801, cat. No. T8309), tenofovir (cat. No. T1649), and sofosbuvir (Cat. No. T6676) were obtained from TargetMol (MA, USA). Recombinant SARS-CoV-2 RdRp His-tag protein (10686-CV-050) was sourced from R&D Systems (MN, USA). SARS-CoV-2 (2019-nCoV) Nsp7-recombinant protein (40617-VNCE) and SARS-CoV-2 Nsp8 protein (40618-VNCE) were procured from Sino Biological (Beijing, China).

Establishment of reporter vector

A gene construct was synthesized, consisting of a ribozyme-ribozyme sequence flanked by NheI and ApaI sites at the 5′ and 3′ termini, with BamHI and XhoI sites inserted between the ribozymes. Additionally, a 3′ UTR of SARS-CoV-2 with BamHI and EcoRI sites, as well as a 5′ UTR of SARS-CoV-2 with NotI and XhoI sites at both ends, were synthesized via Bionics (Seoul, Korea). The synthesized HDV ribozyme-ribozyme was cloned into the pcDNA3.1 vector through subcloning using NheI and ApaI. Subsequently, the FLuc gene was subcloned into EcoRI and NotI within the multiple cloning sites of pcDNA3.1-ribozyme-ribozyme. The 3′ UTR with BamHI and EcoRI sites and the 5′ UTR with NotI and XhoI sites were then cloned into the respective enzyme sites of the pcDNA3.1-ribozyme-FLuc-ribozyme plasmid. This final constructed reporter plasmid contained the 3′ UTR, FLuc, and 5′ UTR genes in sequence and in the reverse direction under the control of the CMV promoter in the pcDNA3.1 vector.

Cell viability in HEK 293 and A549 cells

HEK 293 and A549 cells were seeded in 96-well plates at a density of 4×10^4 cells/well and cultured in DMEM medium supplemented with 10% FBS. Compounds were added at various concentrations and incubated for 24 h. Cell viability was assessed using EZ-Cytox (DoGenBio, Seoul, Korea) according to the manufacturer's instructions. The EZ-Cytox solution, diluted to 1/20 of the culture medium volume, was added to each well and incubated for 40 min in a humidified incubator at 37 °C with 5% CO_2. Optical density was measured at 450 nm and 650 nm using a Synergy H1 Microplate Reader (BioTek Instruments, VT, USA).

Luciferase reporter assay with the calculation of Z-factor

HEK 293 cells were seeded in 100 mm dishes and incubated overnight at 37 °C until reaching 70–80% confluency. Transfection was performed using polyethylenimine as the transfection agent to introduce the reporter vector, either alone or together with strep-tagged SARS-CoV-2 RdRp, Nsp7, Nsp8, or mutant forms of SARS-CoV-2 RdRp. For reporter activity measurements without compound treatment, the transfected cells were incubated at 37 °C for 48 h and subsequently lysed using a cell culture lysis reagent (Promega, WI, USA). For compound-treated reporter assays, the transfected cells were incubated overnight at 37 °C, then split into 48-well plates. Cells were treated with DMSO, remdesivir as a positive control, or other chemical compounds and incubated for an additional 24 h. Subsequently, cell lysis was carried out using a cell culture lysis reagent, and the samples were analyzed using a luciferase assay reagent (Promega, WI, USA). Luminescence and fluorescence measurements were recorded using a Synergy H1™ Hybrid Microplate Reader (Biotek, VT, US).

The formula for calculating the Z-Factor is as follows: $1 - [3(SD_{Negative} + SD_{Positive})/|mean_{Negative} - mean_{Positive}|]$, where SD represents the standard deviation[32]. The luciferase assay was conducted with $n = 30$ for each group.

Preparation of cell lysate and Immunoblotting

The cells were rinsed with phosphate-buffered saline (PBS, pH 7.4) and lysed using a buffer containing 150 mM NaCl, 20 mM tris(hydroxymethyl)aminomethane hydrochloride (Tris-HCl; pH 8.0), 0.5% Triton X-100, 1% glycerol, 1 mM ethylenediaminetetraacetic acid (EDTA), 2 mM phenylmethylsulfonyl fluoride, 10 mM NaF, and 1 mM Na_3VO_4. The lysates were centrifuged at 13,000 rpm at 4 °C for 15 min, and the supernatants were carefully transferred to new tubes.

Protein quantification was performed using the Bradford protein assay (Bio-Rad, CA, USA) following the manufacturer's instructions. The lysates were mixed with 5× sample buffer containing 250 mM Tris-HCl (pH 6.8), 50% glycerol, 10% sodium dodecyl sulfate (SDS), 5% β-mercaptoethanol, and 0.01% bromophenol blue. Samples were boiled at 100 °C for 5 min, separated by SDS-polyacrylamide gel electrophoresis (PAGE, and transferred to nitrocellulose membranes (GE Healthcare, WI, USA). The membranes were blocked with 5% non-fat dried skim milk in 1× Tris-buffered saline with 0.05% Tween 20 (TBST) and incubated overnight at 4 °C with primary antibodies diluted 1:1,000 in 5% bovine serum albumin (BSA) in TBST. After washing three times with 1× TBST, the membranes were incubated with secondary antibodies diluted 1:5,000 in 5% non-fat dried skim milk in 1× TBST at room temperature for 2 h. Target protein bands were visualized using enhanced

chemiluminescence detection reagent (IL, USA), and protein levels were captured and analyzed using LabWorks software (UVP Inc., CA, USA).

Primer: template RNA duplex annealing and primer extension polymerase assay

Primer (5′-[Cyanine5] GCUAUGUGAGAUUAAGAAUU-3′) and template (5′-UUUUUUUUUUAAUUCUUA AUCUCACAUAGC-3′) were synthesized by Bioneer (Daejeon, Korea). Both were dissolved in distilled water to a final concentration of 100 μM. The primer and template were annealed at a molar ratio of 1:1.5 in an annealing buffer containing 10 mM Tris-HCl (pH 8.0), 25 mM NaCl, and 2.5 mM EDTA. This annealing process was conducted at 95 °C for 10 min, followed by gradual cooling to room temperature over several hours.

In the primer extension assay, recombinant SARS-CoV-2 RdRp His-tag protein, SARS-CoV-2 (2019-nCoV) Nsp7-recombinant protein, and SARS-CoV-2 Nsp8 protein were used. The active SARS-CoV-2 RdRp complex was formed by incubating Nsp7 and Nsp8 at equimolar concentrations (50 μM) for 30 min at room temperature. RdRp and additional Nsp8 were then added to achieve a final complex composition of RdRp: Nsp7:Nsp8 in a 1:3:3 ratio, with 0.5 μM of RdRp. For the primer extension polymerase assay, this complex was combined with the annealed primer-template and various concentrations of MePT-S-N-PMe. The reaction was carried out in a buffer containing Tris-HCl (pH 8.0), 10 mM KCl, 1 mM dithiothreitol (DTT), 6 mM $MgCl_2$, and 0.01% Triton-X 100, supplemented with 50 μM ATP. The reaction was incubated for 1 h at room temperature and then quenched by adding 2× RNA loading dye (B0363S; New England Biolabs, MA, USA). The reaction products were separated using 8 M urea-PAGE, visualized with Davinch Auto Chemi & Fluoro imaging (CAS400MF, Davinch K, Seoul, Korea), and analyzed with ImageJ 1.53v (National Institutes of Health, MD, USA).

Expression and purification of Nsp9 protein

To express and purify Nsp9 with a native N-terminus for the NMPylation assay, the pIA1414 plasmid encoding SARS-CoV-2 Nsp9 with an N-terminal His-small ubiquitin-related modifier (SUMO) tag was obtained from Addgene[11]. The plasmid was transformed into *Escherichia coli* BL21 (DE3) CodonPlus-RIL strain, cultured in Luria Bertani broth at 37 °C until the optical density at 600 nm reached 0.6. Protein expression was induced with 0.5 mM isopropyl β-d-1-thiogalactopyranoside, and the culture was incubated at 30 °C for 5 h. Cells were harvested by centrifugation at 5,000 rpm and stored at − 80 °C until purification. The cells were resuspended in a lysis buffer containing 20 mM Tris-HCl (pH 8.0), 150 mM NaCl, and 2 mM β-mercaptoethanol, disrupted by sonication, and the debris was removed by centrifugation at 12,000 rpm for 30 min. The supernatant was loaded onto an open column containing Ni-NTA affinity resin (Cytiva, MA, USA). After washing with the lysis buffer supplemented with 20 mM imidazole (pH 8.0), the His-SUMO tag was cleaved on the column with SUMO protease (PR015; Enzynomics, Daejeon, Korea). The cleaved Nsp9 was passed through a HiTrap Capto Q ImpRes column (Cytiva, MA, USA) pre-equilibrated with the lysis buffer. The flow-through was collected and subjected to size-exclusion chromatography on a HiLoad Superdex 200 16/600 column (Cytiva, MA, USA) equilibrated with a buffer containing 20 mM Tris-HCl (pH 8.0), 150 mM NaCl, 10% (v/v) glycerol, and 2 mM β-mercaptoethanol. The purified Nsp9 protein was concentrated using a centrifugal filter unit (Sartorius, Göttingen, Germany) and stored at − 80 °C.

NMPylation assay

MePT-S-N-PMe (20 and 50 μM) was incubated with 0.5 μM of recombinant SARS-CoV-2 RdRp His-tag protein for 1 h at 4 °C in NMPylation buffer (50 mM HEPES, pH 7.5, 2 mM DTT, and 1 mM $MnCl_2$). The reaction mixture was then incubated with 5 μM of purified Nsp9 and a uridine triphosphate (UTP) mixture (1.7 μM of Fluorescein-12-UTP and 25 μM of UTP) for 30 min at room temperature. The reaction was terminated by adding 5× SDS-PAGE sample buffer containing β-mercaptoethanol and boiling at 95 °C for 5 min. The proteins were loaded onto a 12% SDS-PAGE gel, and fluorescence emitted from Nsp9 was detected using Davinch Auto Chemi & Fluoro imaging. The gel was then stained with Coomassie Brilliant Blue solution (40% methanol, 10% acetic acid, and 0.05% Coomassie Brilliant Blue) to confirm the sizes of the loaded proteins, Nsp9 and RdRp.

Assessment of SARS-CoV-2 replication and cell viability in Vero cells using Immunofluorescence assay

SARS-CoV-2 (βCoV/KOR/KCDC03/2020, NCCP43326, lineage A) was provided by the National Culture Collection for Pathogens. This virus was propagated in Vero cells (CCL-81; ATCC, VA, USA) in DMEM with 2% FBS (Gibco, MA, USA) and 1× antibiotic-antimycotic (Gibco, MA, USA). Cells were grown in T-175 flasks, inoculated with SARS-CoV-2, and incubated for 3 days at 37 °C in a 5% CO_2 environment. The SARS-CoV-2 viruses were harvested and stored at − 80 °C.

To assess the inhibitory effect on SARS-CoV-2 replication, Vero cells were seeded at 1.2×10^4 cells per well in black 384-well μClear plates (Greiner Bio-One, Austria) 24 h before the experiment. MePT-S-N-PMe was serially diluted with DMSO and applied to the cells. The plates were then transferred to a biosafety level 3 isolation facility for viral infection, and SARS-CoV-2 was added at a multiplicity of infection (MOI) of 0.025 and incubated for an additional 24 h. The cells were fixed with 4% paraformaldehyde, immunostained with an antibody against the SARS-CoV-2 N protein, and the nuclei were visualized with DNA fluorochrome Hoechst 33342. Images were acquired using an Operetta CLS high-throughput imaging device (PerkinElmer, Inc., MA, USA) and analyzed with Columbus software (PerkinElmer, Inc., MA, USA) to quantify cell numbers and infection ratios. The total number of cells per well was determined by counting nuclei stained with Hoechst, while the number of infected cells was quantified based on the expression of viral N protein. Cell viability (%) was calculated by normalizing the cell count in each well to the average cell count of the mock group. Antiviral activity was normalized by setting the average infection ratio of mock-infected wells to 100% and that of virus-infected wells treated with 0.5% DMSO to 0% within the same plate. A graph of cell viability and inhibition

of viral replication was fitted by sigmoidal dose-response models using the following equation: Y = bottom + (top – bottom)/[1 + (IC_{50}/X)Hillslope], using Prism7 (GraphPad Software, CA, USA). Half maximal inhibitory concentration (IC_{50}) values were calculated from the normalized activity data set-fitted curves. All IC_{50} and 50% cytotoxic concentration (CC_{50}) values were measured in duplicate, and quality of each assay was controlled by the Z′-factor and the coefficient of variation in percentage.

SARS-CoV-2-NLuc antiviral assay and cell viability in A549-hACE2-TMPRSS2 cells

A549-hACE2-TMPRSS2 cells were purchased from National Institute for Biological Standards and Control and grown at 37 °C with 5% CO_2 in Ham's F-12 K (Kaighn's) medium (Gibco, MA, USA), supplemented with 10% FBS and 2 mg/ml Geneticin (Gibco, MA, USA), 200 µg/ml Hygromycin B (Gibco, MA, USA) and 1× antibiotic-antimycotic.

A549-hACE2-TMPRSS2 cells (1.0×10^4 cells/well) were plated into white 384-well µClear plates. On the next day, 2-fold serial dilution series of MePT-S-N-PMe prepared in DMSO was added to each well and the cells were infected with SARS-CoV-2-NLuc (MOI of 0.01)[69]. The virus used in this assay was the ancestral strain, consistent with that used in the Vero cell. After incubation for 24 h at 37 °C, Nano-Glo® Luciferase Assay System (Promega, WI, USA) was used by adding the luciferase substrate to each well, and luciferase signals were measured using a VICTOR Nivo™ multilabel plate reader (Revvity, MA, USA). Cell viability was measured using the CellTiter-Glo Luminescent Cell Viability Assay (Promega, WI, USA), according to the manufacturer instructions. The relative luciferase signals of the MePT-S-N-PMe-treated groups were normalized to that of non-infection control (set as 0%) and DMSO-treated groups (set as 100%). The plots were generated using Prism6 software (GraphPad, San Diego, CA), and IC_{50} and CC_{50} values were calculated using a nonlinear regression model.

Statistical analyses

All experiments were conducted independently in triplicate. Data are presented as the mean ± SD of three distinct experiments. Statistical analyses were performed using one-way analysis of variance (ANOVA) followed by Dunnett's multiple comparison test using GraphPad Prism 3.0 (GraphPad Software, MA, USA). Statistically significant values were defined as $^{a}p < 0.05$, $^{b}p < 0.01$, and $^{c}p < 0.001$ compared to the reporter vector expressed group; $^{*}p < 0.05$, $^{**}p < 0.01$, and $^{***}p < 0.001$ compared to the reporter vector and RdRp co-expressed group; $^{A}p < 0.001$ compared to the group without reporter vector and RdRp; and $^{\#}p < 0.05$ compared to the group treated with ATP and RdRp complex. Non-significant differences are denoted as "*n.s.*" on the graph.

Data availability

All data generated or analyzed during this study are included in this published article (and its Supplementary Information files).

Received: 17 February 2025; Accepted: 22 May 2025
Published online: 26 May 2025

References

1. Wu, D., Wu, T., Liu, Q. & Yang, Z. The SARS-CoV-2 outbreak: what we know. *Int. J. Infect. Dis.* **94**, 44–48 (2020).
2. Al-Salihi, K. A. & Khalaf, J. M. The emerging SARS-CoV, MERS-CoV, and SARS-CoV-2: an insight into the viruses zoonotic aspects. *Vet. World*. **14**, 190–199 (2021).
3. Sharma, A., Tiwari, S., Deb, M. K. & Marty, J. L. Severe acute respiratory syndrome coronavirus-2 (SARS-CoV-2): a global pandemic and treatment strategies. *Int. J. Antimicrob. Agents*. **56**, 106054 (2020).
4. Gorkhali, R. et al. Structure and function of major SARS-CoV-2 and SARS-CoV proteins. *Bioinform Biol. Insights*. **15**, 11779322211025876 (2021).
5. Yang, H. & Rao, Z. Structural biology of SARS-CoV-2 and implications for therapeutic development. *Nat. Rev. Microbiol.* **19**, 685–700 (2021).
6. Razali, R., Asis, H. & Budiman, C. Structure-Function characteristics of SARS-CoV-2 proteases and their potential inhibitors from microbial sources. *Microorganisms* **9**, 2481 (2021).
7. Yadav, R. et al. Role of structural and Non-Structural proteins and therapeutic targets of SARS-CoV-2 for COVID-19. *Cells* **10**, 821 (2021).
8. Wu, J. et al. SARS-CoV-2 RNA-dependent RNA polymerase as a target for high-throughput drug screening. *Future Virol.* **18**, 51–62 (2023).
9. Kirchdoerfer, R. N. & Ward, A. B. Structure of the SARS-CoV nsp12 polymerase bound to nsp7 and nsp8 co-factors. *Nat. Commun.* **10**, 2342 (2019).
10. Chen, J. et al. Structural basis for Helicase-Polymerase coupling in the SARS-CoV-2 Replication-Transcription complex. *Cell.* **182**, 1560–1573 (2020).
11. Wang, B., Svetlov, D. & Artsimovitch, I. NMPylation and de-NMPylation of SARS-CoV-2 nsp9 by the NiRAN domain. *Nucleic Acids Res.* **49**, 8822 (2021).
12. Ahmad, J., Ikram, S., Ahmad, F., Rehman, I. U. & Mushtaq, M. SARS-CoV-2 RNA dependent RNA polymerase (RdRp) – A drug repurposing study. *Heliyon* **6**, e04502 (2020).
13. Wang, R., Hozumi, Y., Yin, C. & Wei, G. W. Decoding SARS-CoV-2 transmission and evolution and ramifications for COVID-19 diagnosis, vaccine, and medicine. *J. Chem. Inf. Model.* **60**, 5853–5865 (2020).
14. Malone, B., Urakova, N., Snijder, E. J. & Campbell, E. A. Structures and functions of coronavirus replication–transcription complexes and their relevance for SARS-CoV-2 drug design. *Nat. Rev. Mol. Cell. Biol.* **23**, 21–39 (2022).
15. Peng, Q. et al. Structural and biochemical characterization of the nsp12-nsp7-nsp8 core polymerase complex from SARS-CoV-2. *Cell Rep.* **31**, 107774 (2020).
16. Uppal, T. et al. Screening of SARS-CoV-2 antivirals through a cell-based RNA-dependent RNA polymerase (RdRp) reporter assay. *Cell Insight*. **1**, 100046 (2022).
17. Tian, L. et al. Molnupiravir and its antiviral activity against COVID-19. *Front. Immunol.* **13**, 855496 (2022).
18. Jonsdottir, H. R. et al. Molnupiravir combined with different repurposed drugs further inhibits SARS-CoV-2 infection in human nasal epithelium in vitro. *Biomed. Pharmacother*. **150**, 113058 (2022).

19. Hasan, M. K. et al. Structural analogues of existing anti-viral drugs inhibit SARS-CoV-2 RNA dependent RNA polymerase: A computational hierarchical investigation. *Heliyon* **7**, e06435 (2021).
20. Xue, Y. et al. Repurposing clinically available drugs and therapies for pathogenic targets to combat SARS-CoV-2. *MedComm.* **4**, e254 (2023).
21. Elfiky, A. A. Ribavirin, Remdesivir, Sofosbuvir, Galidesivir, and Tenofovir against SARS-CoV-2 RNA dependent RNA polymerase (RdRp): A molecular Docking study. *Life Sci.* **253**, 117592 (2020).
22. Wang, X. et al. Combination of antiviral drugs inhibits SARS-CoV-2 polymerase and exonuclease and demonstrates COVID-19 therapeutic potential in viral cell culture. *Commun. Biol.* **5**, 154 (2022).
23. Chang, C. W. et al. A newly engineered A549 cell line expressing ACE2 and TMPRSS2 is highly permissive to SARS-CoV-2, including the Delta and Omicron variants. *Viruses* **14**, 1369 (2022).
24. Pandamooz, S. et al. Experimental models of SARS-CoV-2 infection: possible platforms to study COVID-19 pathogenesis and potential treatments. *Annu. Rev. Pharmacol. Toxicol.* **62**, 25–53 (2022).
25. Burhan, E. et al. Evaluation of safety and effectiveness of Remdesivir in treating COVID-19 patients after emergency use authorization study. *Front. Pharmacol.* **14**, 1205238 (2023).
26. Zibat, A. et al. N4-hydroxycytidine, the active compound of Molnupiravir, promotes SARS-CoV-2 mutagenesis and escape from a neutralizing nanobody. *iScience* **26**, 107786 (2023).
27. Xu, X. et al. An update on inhibitors targeting RNA-dependent RNA polymerase for COVID-19 treatment: promises and challenges. *Biochem. Pharmacol.* **205**, 115279 (2022).
28. Dwivedy, A. et al. Characterization of the NiRAN domain from RNA-dependent RNA polymerase provides insights into a potential therapeutic target against SARS-CoV-2. *PLOS Comput. Biol.* **17**, e1009384 (2021).
29. Weisberg, E. et al. Repurposing of kinase inhibitors for treatment of COVID-19. *Pharm. Res.* **37**, 167 (2020).
30. Mondal, S. K. et al. In Silico analysis of RNA-dependent RNA polymerase of the SARS-CoV-2 and therapeutic potential of existing antiviral drugs. *Comput. Biol. Med.* **135**, 104591 (2021).
31. Geerling, E. et al. Roles of antiviral sensing and type I interferon signaling in the restriction of SARS-CoV-2 replication. *iScience* **25**, 103553 (2022).
32. Min, J. S., Kim, G. W., Kwon, S. & Jin, Y. H. A Cell-Based reporter assay for screening inhibitors of MERS coronavirus RNA-Dependent RNA polymerase activity. *J. Clin. Med.* **9**, 2399 (2020).
33. Lee, J. C. et al. A cell-based reporter assay for inhibitor screening of hepatitis C virus RNA-dependent RNA polymerase. *Anal. Biochem.* **403**, 52–62 (2010).
34. Yan, W., Zheng, Y., Zeng, X., He, B. & Cheng, W. Structural biology of SARS-CoV-2: open the door for novel therapies. *Signal. Transduct. Target. Ther.* **7**, 26 (2022).
35. Min, J. S., Kwon, S. & Jin, Y. H. SARS-CoV-2 RdRp inhibitors selected from a Cell-Based SARS-CoV-2 RdRp activity assay system. *Biomedicines* **9**, 996 (2021).
36. Begum, F., Srivastava, A. K. & Ray, U. Repurposing nonnucleoside antivirals against SARS-CoV2 NSP12 (RNA dependent RNA polymerase): in silico-molecular insight. *Biochem. Biophys. Res. Commun.* **571**, 26–31 (2021).
37. Stevens, L. J. et al. Mutations in the SARS-CoV-2 RNA-dependent RNA polymerase confer resistance to Remdesivir by distinct mechanisms. *Sci. Transl Med.* **14**, eabo0718 (2022).
38. Park, G. J. et al. The mechanism of RNA capping by SARS-CoV-2. *Nature* **609**, 793–800 (2022).
39. Santoro, M. G. & Carafoli, E. Remdesivir: From Ebola to COVID-19. *Biochem. Biophys. Res. Commun.* **538**, 145–150 (2021).
40. Pruijssers, A. J. et al. Remdesivir inhibits SARS-CoV-2 in human lung cells and chimeric SARS-CoV expressing the SARS-CoV-2 RNA polymerase in mice. *Cell. Rep.* **32**, 107940 (2020).
41. Kokic, G. et al. Mechanism of SARS-CoV-2 polymerase stalling by Remdesivir. *Nat. Commun.* **12**, 1–7 (2021).
42. Eastman, R. T. et al. A review of its discovery and development leading to emergency use authorization for treatment of COVID-19. *ACS Cent. Sci.* **6**, 672–683 (2020). Remdesivir.
43. Pirzada, R. H., Haseeb, M., Batool, M., Kim, M. & Choi, S. Remdesivir and Ledipasvir among the FDA-Approved antiviral drugs have potential to inhibit SARS-CoV-2 replication. *Cells* **10**, 1052 (2021).
44. Singh, A. K., Singh, A., Singh, R. & Misra, A. An updated practical guideline on use of molnupiravir and comparison with agents having emergency use authorization for treatment of COVID-19. *Diabetes Metab. Syndr. Clin. Res. Rev.* **16**, 102396 (2022).
45. Kabinger, F. et al. Mechanism of molnupiravir-induced SARS-CoV-2 mutagenesis. *Nat. Struct. Mol. Biol.* **28**, 740–746 (2021).
46. Jenh, A. M., Thio, C. L. & Pham, P. A. Tenofovir for the treatment of hepatitis B virus. *Pharmacother J. Hum. Pharmacol. Drug Ther.* **29**, 1212–1227 (2009).
47. Lin, M. V. & Chung, R. Recent FDA approval of Sofosbuvir and Simeprevir. Implications for current HCV treatment. *Clin. Liver Dis.* **3**, 65–68 (2014).
48. Zhao, J. et al. A cell-based assay to discover inhibitors of SARS-CoV-2 RNA dependent RNA polymerase. *Antiviral Res.* **190**, 105078 (2021).
49. Yang, M. & Xu, X. Important roles of transporters in the pharmacokinetics of anti-viral nucleoside/nucleotide analogs. *Expert Opin. Drug Metab. Toxicol.* **18**, 483 (2022).
50. Kamzeeva, P. N., Aralov, A. V., Alferova, V. A. & Korshun, V. A. Recent advances in molecular mechanisms of nucleoside antivirals. *Curr. Issues Mol. Biol.* **45**, 6851–6879 (2023).
51. Gallois-Montbrun, S. et al. Broad specificity of human phosphoglycerate kinase for antiviral nucleoside analogs. *Biochem. Pharmacol.* **68**, 1749–1756 (2004).
52. Elgohary, M. A. S. et al. Efficacy of Sofosbuvir plus Ledipasvir in Egyptian patients with COVID-19 compared to standard treatment: a randomized controlled trial. *J. Med. Life.* **15**, 350 (2022).
53. Blair, H. A. Remdesivir: A review in COVID-19. *Drugs* **83**, 1215–1237 (2023).
54. Liang, Y. et al. Adverse events associated with Molnupiravir: a real-world disproportionality analysis in food and drug administration adverse event reporting system. *Front. Pharmacol.* **14**, 1–11 (2023).
55. Polo, R. et al. Daily Tenofovir disoproxil fumarate/emtricitabine and hydroxychloroquine for pre-exposure prophylaxis of COVID-19: a double-blind placebo-controlled randomized trial in healthcare workers. *Clin. Microbiol. Infect.* **29**, 85–93 (2023).
56. Pillaiyar, T. & Laufer, S. Kinases as potential therapeutic targets for Anti-coronaviral therapy. *J. Med. Chem.* **65**, 955–982 (2022).
57. Boytz, R. M. et al. Anti-SARS-CoV-2 activity of targeted kinase inhibitors: repurposing clinically available drugs for COVID-19 therapy. *J Med. Virol.* **95**, e28157 (2023).
58. Shannon, A. et al. A dual mechanism of action of AT-527 against SARS-CoV-2 polymerase. *Nat. Commun* **131**(13), 7–9 (2022).
59. Gandek, T. B., van der Koog, L. & Nagelkerke, A. A. Comparison of cellular uptake mechanisms, delivery efficacy, and intracellular fate between liposomes and extracellular vesicles. *Adv Healthc. Mater.* **12**, e2300319 (2023).
60. Nishino, K., Yamasaki, S., Nakashima, R., Zwama, M. & Hayashi-Nishino, M. Function and inhibitory mechanisms of multidrug efflux pumps. *Front. Microbiol.* **12**, 737288 (2021).
61. He, X. et al. Generation of SARS-CoV-2 reporter replicon for high- throughput antiviral screening and testing. *Proc. Natl. Acad. Sci. U.S.A* **118**, e2025866118 (2021)
62. Ahmad, H. A. et al. Signaling Pathways in Drug Development. *IntechOpen.* https://doi.org/10.5772/INTECHOPEN.114041. (2024).
63. Chawla, S. et al. Gene expression based inference of cancer drug sensitivity. *Nat. Commun.* **13**, 5680 (2022).

64. Bahia, D., Satoskar, A. R. & Dussurget, O. Editorial: Cell signaling in host–Pathogen interactions: the host point of view. *Front. Immunol.* **9**, 221 (2018).
65. Wilamowski, M. et al. Transient and stabilized complexes of Nsp7, Nsp8, and Nsp12 in SARS-CoV-2 replication. *Biophys. J.* **120**, 3152–3165 (2021).
66. Gordon, D. E. et al. A SARS-CoV-2 protein interaction map reveals targets for drug repurposing. *Nature* **583**, 459–468 (2020).
67. Chary, A. Culturing human lung adenocarcinoma cells in a Serum-Free environment. *Methods Mol. Biol.* **2645**, 165–172 (2023).
68. Chary, A. et al. Maximizing the relevance and reproducibility of A549 cell culture using FBS-free media. *Toxicol. Vitr.* **83**, 105423 (2022).
69. Rihn, S. J. et al. A plasmid DNA-launched SARS-CoV-2 reverse genetics system and coronavirus toolkit for COVID-19 research. *PLOS Biol.* **19**, e3001091 (2021).

Author contributions
E.K, H.Y, and S.C. conceptualized this study. E.K. and H.Y. wrote and revised the original draft. E.K., H.Y., and J.L. performed data collection, analysis, and interpretation. J.A.L. and S.K conducted virus-related experiments, analyzed the data, and contributed to its interpretation. I.J. and D.G.J purified and provided protein. S.B.H. provided resources. E.K., H.Y., and S.C. curated the data. S.C. supervised and obtained the funding. All authors have read and agreed to the published version of the manuscript.

Funding
This research was supported by National Research Foundation of Korea (NRF) grants, funded by the Korea government (MSIT) (2021M3E5E3080847, 2021R1A2C1011196, RS-2022-NR067509, and RS-2024-00398073).

Declarations

Competing interests
The authors declare no competing interests.

Additional information
Supplementary Information The online version contains supplementary material available at https://doi.org/10.1038/s41598-025-03813-y.

Correspondence and requests for materials should be addressed to S.C.